PROCEEDINGS A

royalsocietypublishing.org/journal/rspa

Review

Cite this article: Leone G *et al*. 2021 Muography as a new complementary tool in monitoring volcanic hazard: implications for early warning systems. *Proc. R. Soc. A* **477**: 20210320.
https://doi.org/10.1098/rspa.2021.0320

Received: 13 April 2021
Accepted: 6 October 2021

Subject Areas:
volcanology, geophysics

Keywords:
muography, volcanic hazard, volcano-monitoring

Author for correspondence:
Giovanni Leone
e-mail: giovanni.leone@uda.cl

Muography as a new complementary tool in monitoring volcanic hazard: implications for early warning systems

Giovanni Leone[1,2,†], Hiroyuki K. M. Tanaka[2,3,4], Marko Holma[2,5,6,7], Pasi Kuusiniemi[2,6,7], Dezső Varga[8], László Oláh[2,3,4], Domenico Lo Presti[2,9,10], Giuseppe Gallo[10], Carmelo Monaco[11,12], Carmelo Ferlito[11,12], Giovanni Bonanno[13], Giuseppe Romeo[13], Lee Thompson[2,14,15], Kenji Sumiya[2,16], Sara Steigerwald[2] and Jari Joutsenvaara[2,5,6,7]

[1]Instituto de Investigación en Astronomía y Ciencias Planetarias, Universidad de Atacama, Chile, Western South America
[2]Virtual Muography Institute, Global, Tokyo, Japan
[3]International Muography Research Organization (MUOGRAPHIX), The University of Tokyo, Japan
[4]Earthquake Research Institute, The University of Tokyo, 1-1-1 Yayoi, Bunkyo, Tokyo 113-0032, Japan
[5]Kerttu Saalasti Institute, University of Oulu, Finland
[6]Muon Solutions Oy, Finland
[7]Arctic Planetary Science Institute, Rovaniemi, Finland
[8]Wigner Research Centre for Physics, Hungary
[9]Dipartimento di Fisica e Astronomia "E. Majorana", Universitá di Catania, Via S. Sofia 64, 95123, Italy
[10]Dipartimento di Fisica, Università di Catania, Via S. Sofia 64, 95123 Catania, Italy
[11]Dipartimento di Scienze Biologiche, Geologiche e Ambientali, Universitá di Catania, Corso Italia 57, 95129 Catania, Italy
[12]Istituto Nazionale di Geofisica e Vulcanologia, Osservatorio Etneo, 95125 Catania, Italy
[13]INAF, Osservatorio Astrofisico di Catania, Via S. Sofia 78, 95123 Catania, Italy

[†]Present address: Instituto de Investigación en Astronomía y Ciencias Planetarias, Universidad de Atacama, Copiapó, Chile.

THE ROYAL SOCIETY PUBLISHING

[14]Department of Physics and Astronomy, University of Sheffield, UK
[15]Geoptic Ltd., UK
[16]Kansai University, Japan

GL, 0000-0003-1479-9039; HKMT, 0000-0002-3816-1630

Muography uses muons naturally produced in the interactions between cosmic rays and atmosphere for imaging and characterization of density differences and time-sequential changes in solid (e.g. rocks) and liquid (e.g. melts ± dissolved gases) materials in scales from tens of metres to up to a few kilometres. In addition to being useful in discovering the secrets of the pyramids, ore prospecting and surveillance of nuclear sites, muography successfully images the internal structure of volcanoes. Several field campaigns have demonstrated that muography can image density changes relating to magma ascent and descent, magma flow rate, magma degassing, the shape of the magma body, an empty conduit diameter, hydrothermal activity and major fault lines. In addition, muography is applied for long-term volcano monitoring in a few selected volcanoes around the world. We propose using muography in volcano monitoring in conjunction with other existing techniques for predicting volcanic hazards. This approach can provide an early indication of a possible future eruption and potentially the first estimate of its scale by producing direct evidence of magma ascent through its conduit in real time. Knowing these issues as early as possible buy critically important time for those responsible for the local alarm and evacuation protocols.

royalsocietypublishing.org/journal/rspa *Proc. R. Soc. A* **477**: 20210320

1. Introduction

A muon is an elementary particle similar to the electron but with a much greater mass (about 207 times greater). Its corresponding antiparticle, called antimuon, has a positive charge, which explains why it is also known as the positive muon. Muons—be they negative or positive—form the basis for muography, a novel method that uses the detection of muons that are a major component of extensive air showers formed in the upper atmosphere from collisions between high-energy cosmic-ray particles and atmospheric nuclei [1,2]. A single cascade may consist of millions of particles [1]. Most muons reaching the Earth's surface originate from a constant flux of medium to high-energy (from 100 MeV to 10^{20} eV) cosmic-ray particles of galactic origin as observed by Cherenkov or fluorescence light apparatus [3]. Therefore, they can be considered as a nearly time-independent, continuous, particle source. Muons are unstable, decaying into electrons and neutrinos with a mean lifetime of 2.2 μs; muons' larger mass than electrons, the absence of strong nuclear interactions, negligible probability of producing electromagnetic cascades and relatively small energy losses by ionization make them a good tool for imaging of large-scale structures on Earth [4]. Analysis techniques have been developed for muons that provide three levels of purity versus efficiency [5], following the criteria in [6]. For muography, all particles except muons are background noise and hence potentially harmful for particle identification [7]. However, apart from muons, all these particles are naturally filtered out once they hit the upmost layers of soil or rock. Consequently, the high-energy muons can penetrate deeper regions underground than most particles [8]. The aim of this paper is to review how muography could be useful in monitoring volcanic hazards as a standard addition to the state-of-the-art volcano monitoring systems.

2. Volcano monitoring systems

Forecasting violent volcanic eruptions is the Holy Grail for applied volcanology. Volcanic monitoring requires a deep understanding of the volcanic processes related to every single

volcanic centre within the given volcanic system [9]. The appraisal and mitigation of volcanic hazards also require a deep understanding of volcano-specific histories and tracking magma movement in real time [10]. For this reason, a multidisciplinary approach is often applied to volcanic monitoring, including at least some of the following methods:

- field observation integrated with space-borne data, interferometric synthetic aperture radar (InSAR) using ENVISAT-ASAR and ALOS-PALSAR (although now out of service), RADARSAT-2, TerraSAR-X and TanDEM-X imagery [11],
- ground-based, airborne and space-borne measurements of gas emissions (e.g. SO_2, H_2S and CO_2) [12–16],
- radio-equipped human observers [17],
- seafloor and land observation [18–22],
- live camera images displaying the textural and compositional analysis of the material produced during and after eruptions [23,24],
- regular sampling and studies of ash [25–27],
- GPS and seismic networks integrated with magnetic stations and infrared satellite images [28–31],
- acoustic and thermal records [32] and
- infrasonic and Doppler radar measurements; infrasonic microphones (one Larsen-Davis, 3 dB at 0.25 Hz and two McChesney, *ca* 2.5 Hz) and Doppler radar measurements using modified radar system operating at 1 Hz of sampling frequency [33,34].

However, these existing techniques (including muography) have their own shortcomings that we briefly mention here thanks to a previous analysis of Takahashi [35] for seismic methods and to the above-mentioned literature for the other methods: (i) seismic refraction methods may not be useful in case of velocity inversions (i.e. velocity does not increase with depth) or in case of the 'blind zone problem' when some layers hinder the seismic first arrivals; (ii) satellites are not always available on top of the target due to their orbital motion; (iii) airborne observations are not recommendable for security reasons in case of a sudden eruption with ash emissions; (iv) same security reasons apply to radio-equipped human observers; (v) muography can observe targets that are located above (and not below) the detector; (vi) infrasonic methods are able to deliver warnings more than 1 h before the eruption [36], which is more or less the same time scale reported in real-time tracking by means of ground deformation [37]. Clearly, this time scale does not allow enough time to evacuate the population of even a small nearby centre, let alone a larger centre. Seismic precursors are not reliable more than few days before the eruptive event [38], and, unless when strictly necessary, it is quite impractical to evacuate entire populations for days.

Volcanoes are generally surrounded by higher geological structures shielding cosmic ray flux. Furthermore, for land-based muography, potential observation points depend on accessibility and infrastructures. For example, Tanaka [39] examined two possible observation points at the foot of Unzen volcano, Japan. However, land-based muography from these points were impossible due to the additional rock thickness, hence substantial reduction of the penetrating muon flux. Airborne muography has three major advantages over land-based muography: (a) availability of electricity inside the aircraft; (b) aviation-based fast transportation and installation of the detector to the site and (c) the detector can be in the optimum position for collection of muon events. Condition (c) in particular shortens the time required for obtaining images. Tanaka [39] conducted the first airborne muography measurement (figure 1), and the internal structure of the Heisei-Shinzan lava dome of Unzen volcano was imaged in 2.5 h. This methodology offered a fast and reliable way to obtain data in a reasonable time. However, it is not universally applicable to all the various specific cases of volcanic alerts, which have each their own peculiar evolution in time.

The comparative cost of muography with the other geophysical methods shows other shortcomings. Commercial application of muon tomography is currently gaining momentum in the mineral exploration phase of the mining industry, where it is of paramount importance first

Figure 1. Airborne muography observations at Unzen volcano, Japan [39]. (*a*) Panoramic view of the volcano with the position of the helicopter carrying the instrument, the white rectangle indicates the position of the helicopter; (*b*) blow-up image of the helicopter seen in (*a*); (*c*) helicopter without instrument; (*d*) helicopter loaded with the instrument. (Online version in colour.)

to discover where the mineral deposits of interest are before the mining can even be considered as a possibility. In mineral exploration, the alternative for the different conventional and emerging geophysical methodologies and field geological methods is drilling with diamond-tipped drills, which usually gives a core sample to analyse. Drilling typically costs around $200–$500 per metre, and usually there is the need to drill at some constant distance, say, around 100–500 m. So, the price for drilling typically goes around $20 k–$100 k per hole. However, there is no guarantee that one single drill hole will find a deposit, often many holes need to be drilled. In an interesting report from a gold mine[1], two drill holes, totalling 3500 m in length (estimated cost $700 k–$1.75 M) were used for exploration.

The cost of muography stands mainly in the construction of the detectors, each one around $250 k, but then there is no need for heavy transport or consumables (e.g. drilling tips). The salary of an operator could reach $100–$200 per day, which is much less than the $200–$500 per metre of the drilling, and the area of coverage of muography is much higher than that covered by simple drilling. Also, the muon tomography equipment is reusable and can be used many times for many survey campaigns—this is a very important point when comparing it with drilling. Other techniques can be used, chemical sampling, etc., but most of these are done in addition to drilling.

Nuclear emulsion, plastic-scintillation and gaseous detectors can be used for muographic observations. The choice of the detectors depends on the availability of space and infrastructure. Nuclear emulsion does not require electric power. Scintillation and gaseous detectors require electric power. In volcano muography, the detector size ranges from several thousand cm^2 [39] to approximately 10 m^2 [40] (figure 2). In general, larger detectors are required when the distance between the detector and the target is longer. For example, Tanaka *et al.* [39] used an approximately 0.5 m^2 detector since this distance was only 200 m. On the other hand, Oláh *et al.* [40] needed a detection area of approximately 8 m^2 since this distance was approximately 3 km.

We propose to integrate muography observations exactly when the seismic precursor becomes reliable so that a complementary monitoring of a potentially dangerous eruption can take place. A good scheduling trade-off between collecting early warning data and response of the

[1]See https://s23.q4cdn.com/277467366/files/doc_news/archive/NR-2019-06-05.pdf.

Figure 2. Photograph of three multi-wire proportional chamber-based muography observation system (MMOS) [40]. Eleven MMOS operated in the Sakurajima Muography Observatory during 2021. The MMOS covers a surface of 8.25 m^2. (Online version in colour.)

population to the warning is imperative to establish an optimum alarm system [41]. Furthermore, only the results of the data analysis of stages relatively close to the possible timeframe of an eruption are integrated according to alarm protocols and subsequently disseminated to the authorities according to the scheme adopted for volcanic warnings [42]. Despite various methods

are useful to analyse and quantify the parameters of the precursors of eruptions and those of the ongoing eruption, uncertainties on time scales relating to the development of the eruption still remain and hamper decision-makers in public warnings [43]. It is hence obvious that our societies need proper warning systems able to detect volcanic eruptions as early as possible thus allowing evacuation procedures in a timely and safe manner.

The experience acquired during the 2010 eruption of Merapi volcano in Indonesia showed that 81% of the population was effectively evacuated a day after issuing the warning. However, even if the evacuation was considered a success, the study of the evacuation management identified several areas for further improvement [44]. The experience acquired from the devastating eruption of the closed-vent Mt Pinatubo volcano (high-viscosity dacitic and andesitic magmas) in June 1991 in western Luzon, Philippines, showed that an effective five-level warning and evacuation system, issued slightly more than a month after the first signs of the reawakening of the volcano, was effective in fixing a permanent zone of prohibition at a radius of 10 km from the volcano [45]. Although these experiences showed a positive response from the authorities and the populations involved, uncertainties and controversies still remain. Decisions are often taken in too short time with limited information [46,47]. The stakes are high: for example, the authorities responsible for monitoring Vesuvius and the surrounding areas in Naples, Italy, have the responsibility to protect a population of about 600 000 people living within the danger zone of the volcano [48].

Based on the study of the 288 most explosive eruptions for which we have adequate data, Siebert *et al*. [49] provide compelling evidence that 52% of the eruptions reached their paroxysmal climax within the first week. However, 42% of the eruptions reached this stage within a day after the eruption began. It is even more staggering that half of these first-day paroxysms took only about an hour from the start of eruption to reach their culmination. For a volcano monitoring system to be as useful as possible in early forecasting and hazard warning system, it has not only to be reliable in evaluating risk levels correctly, but also able to provide notes of alarm as quickly as possible. Nevertheless, in principle, it remains difficult if not impossible to get completely rid of false alarms [50,51]. However, if there are too many false alarms, the general public's perception of volcanic risks may erode, and their behaviour in the face of legitimate volcanic threats may consequentially put them at risk [52]. It is also important to consider that evacuations are cultural, social, political and economic issues [53]. We demonstrate in this paper how volcanic hazard monitoring systems could benefit from muography. In some cases, these benefits may be particularly useful for those monitoring systems of volcanoes that currently are in their long-dormant stage and those that are currently less active.

3. The economic impact of volcanic hazards on aviation safety and business

Available studies on the economic impact of volcanic hazards on the aviation business report losses ranging from 5 to 35 million US dollars for longer volcanic episodes, with minimum amounts of approximately $20 k for every 6 min of air traffic disruption [54]. Much worse was the $1.7 billion loss of revenues due to air traffic disruption followed by the eruption of the Eyjafjallajökull volcano in Iceland in April 2010 [55]. These economic losses were, in fact, more than the total economic damage caused to business activities by all volcanic eruptions combined in the whole decade of the 1990s worldwide [56]. So, given that the cost of volcanic hazards is definitely high, both in terms of human life and economic loss, a timely warning system aimed at reducing logistical and economic inconveniences is in order.

The ash released in volcanic eruptions is a source of major trouble for any air traffic since an accumulation of a few millimetres of ash on the ground is already sufficient to close an airport [57]. Hence, no matter how accurate the prediction system of a volcano eruption is sometimes closing the airports and suspending business activities (including tourism) due to ongoing eruptions is the only viable option. Indeed, volcanic ash composes a significant disruption threat to critical infrastructure services such as aviation; of course, volcanic ash also has devastating effects on the environment and other infrastructures [58]. For example, the Yogyakarta airport in Indonesia was

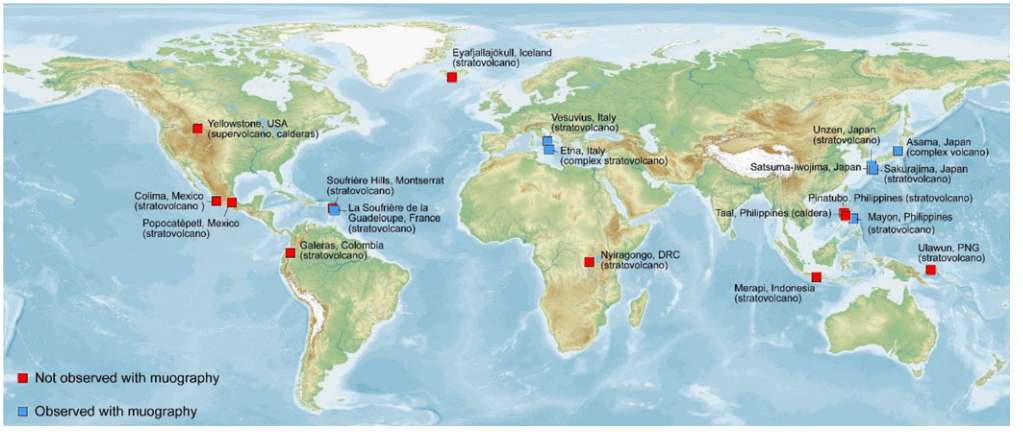

Figure 3. World map with some of the most dangerous volcanoes. Blue and red dots indicate volcanoes observed and not observed with muography, respectively. There are some other muographically studied somewhat less dangerous volcanoes (e.g. in Colombia) but these are omitted for clarity reasons. (Online version in colour.)

closed for 15 days during the eruption of the Merapi volcano in 2010 [59]. Ash dispersed in the atmosphere provokes serious consequences for air traffic safety and other business activities [60]. These situations occur around Mt Etna, Sicily, Italy [28] and have been considered as a major risk in a hypothetical eruption of Mt Somma–Vesuvius [61].

4. Current uncertainties in volcanic hazard analysis

The analysis of volcanic risks is a very complex task given the spectrum of multiple types of hazards (e.g. earthquakes, lava, flank collapses, lahars, debris flows, ash clouds and pyroclastic density currents) and the interwoven cultural, societal, technological and economic vulnerabilities in our societies. Additionally, the uncertainties associated with both the hazards and the effects of cascading hazards together with their impacts on nearby populations require accurate description [47]. Indeed, the reality at many active volcanoes is very complex [62]. We have drawn a map of some known dangerous volcanoes in figure 3 in which we have indicated those already monitored with muography.

The data needed to fully analyse volcanic risks are often insufficiently or inaccurately catalogued or even totally lacking, while it is also true that the risks are dynamic and constantly shifting during volcanic unrest, eruption and after the eruption [63]. In addition, no comprehensive methods for vulnerability and risk assessment are widely accepted and, while some models identify individual interactions between the volcanic hazards and physical vulnerability [64–66], the limited analyses on the multiple dimensions of vulnerabilities obscures our understanding of the real volcanic risks [67].

The UN Sendai Framework for Disaster Risk Reduction 2015–2030 recognizes that a better understanding of risks in all their dimensions is needed for effective risk reduction [68]. Hence, the need for a new generation of approaches to volcanic risk analysis is clear. Although the current methods of volcanic hazard monitoring have been effective in guiding the authorities to manage the various crises seen so far, there is always room for further improvements.

5. The optimal time scale for volcano early warning systems

According to Fournier D'Albe [69], the time scale of the social response to pre-eruption planning can be divided into three phases: alert, readiness and evacuation. The first phase (alert) may last anywhere between 15 and 5 days before the eruption, the second from 5 to 2 days and the third

from 2 days to 1 day [69]. Considering that these numbers have already been verified by the above-mentioned experiences acquired during the Merapi and Mt Pinatubo eruptions, it is clear that an alert system supported by continuous monitoring must be active in the range of a week to two days before the possible eruption. Moreover, the predetermined and drilled evacuation plan must be accomplished within less than 2 days before the eruption truly gains strength. These numbers must also take into account the specific characteristics of the given volcanic hazard zone and the logistic plan of evacuation that depends, among other things, on the available infrastructures (i.e. roads, civil protection equipment, transports available, etc.)

6. Muography as a monitoring tool for volcanoes

Among the various techniques of volcanic monitoring, muography is unique as it is based on astroparticle physical phenomena and technology that differs from those used in conventional geophysics. Muons passing through a geological material lose energy through the excitation and ionization of atoms (due to collisions) and photonuclear interaction, which produce a deflection of the muons from their original trajectories [70]. The attenuation of the energy and the deviation of the effective trajectory of the atmospheric muons crossing a dense medium (e.g. a volcanic edifice, orebody, etc.) are thus observed to reconstruct an integrated density model of the object, which can be, for example, the internal structure of a volcano [71].

In rock imaging, the higher the density differences are, the better is the distinguishing capability of muography. The absorption of muons is the lowest on the top of a volcano where the thickness of a rock column is at its minimum. In other words, muons come across the summit of a volcano in an easier way than they do at its broader base. In this regard, void spaces like conduits or empty magma chambers are relatively easy to detect as they distinguish themselves as low-density objects enclosed by the denser host rocks. Magma follows the same principle, i.e. the higher the density difference between the magma and its surrounding rock the better is the spatial resolution (or image definition) in muographs. The measurement duration for a survey to reach the required statistical significance can be tweaked by adjusting the surface area of the detector: faster data acquisition is possible by a proportional increase of the sensitive area of the detector.

Muography applications feature a remarkably diverse range of requirements and conditions; therefore, a careful assessment of the given objective is needed to find the 'best' type. The choice is often guided by the availability of a reasonable option, and not to find the 'best'. Owing to the ultimate limiting factor of the cosmic particle flux, there is a general rule: one should try to use the largest possible detection area. In addition, there may be practical limitations such as available space, or the size of the access route. Once the limitations and measurement conditions and required precision (angular resolution, necessary detector area) are understood, there may be various detector options which may or may not fit the project budget. Some of the conditions may correlate: if the muon trajectory is short because of space limitation, the required angular resolution can only be reached if the position resolution increases, which may increase cost and complexity. A muographic image is represented as a function of elevation (or zenith) and azimuth angles. The minimum size of these angles defines the maximum definition of the muographic image, and it relies on the spatial (or positioning) resolution of the detector plane and the distance between these planes. Since the power to resolve the target volume depends on this maximum definition and the distance between the detector and target, the measurement time required for recording a given number of muon counts from a given section of the target volume is proportional to the size of the detector, and inversely proportional to the square of the distance between the detector and target. There are two basic types of measurements from the point of view of background (noise) relative to the muons that penetrate the region of interest (signal). In underground measurements [72], below 10 m, all types of cosmic backgrounds are efficiently suppressed; therefore, a rather light-weight tracking system will work well. If the detector is on the surface, which is the case for volcanology, a much larger background is to be dealt with [73]. The background contains a complicated mixture of low energy hadrons,

electrons, as well as muons from hadronic interactions. The background consists of multi-particle showers as well [72]. On the surface, the background reduction can be achieved using passive materials like 'absorber' or 'scatterer' material layers, i.e. lead and polyethylene shielding (e.g. [7]). Active methods include using sophisticated tracking to separate the muon tracks from the soft component tracks. Time of flight (ToF) systems allow the rejection of hits that did not occur in the right sequence. Additionally, ToF analysis can be used to reject tracks created by muons coming from the opposite direction [73]. Hybrid detectors, consisting of several different detection technologies, could also be beneficial. For example, a scintillator detector and water Cherenkov detectors are combined in the Muon telescope (MuTe) developed by Jesús Peña-Rodríguez *et al.*[2] The hodoscope made from scintillators is used as a tracking detector, while the Cherenkov detector measures the energy loss of the crossing particles. Together with ToF and energy deposit rejection, the background can be reduced significantly as up to 36% of events originated from the electrons and positrons, and 34% originated from muons, can be rejected. The revolutionary improvements in muography applications are due to improvement in understanding the measurement possibilities, and improvements in technology.

A constraint of muographic observation is that the time required to resolve a given density variation should not exceed the period of volcanological phenomena which can cause the contrast in the average density length of the volcanic edifice. The N number of counts for muons that are measured with an F flux in a muographic observation system with an acceptance of A_{MOS} during a data collection period of Δt is quantified as follows:

$$N = A_{\mathrm{MOS}} \times \Delta t \times F \tag{6.1}$$

where A_{MOS} acceptance incorporates the directional-dependent covered solid angle, detector surface area and detection efficiency. The ΔL density length contrast appears in the variation of the number of muon counts $\Delta N(L, \Delta L)$ has to be larger than the uncertainty of the number of tracks with standard deviation (s.d.) units in case of sufficient large N (greater than 30). One can give a first-order estimation for the expected time of data collection required to observe a given average density length variation with given standard deviations after a given density length with the application of a given detector acceptance by inserting equation 1 into the observation condition [74]:

$$\Delta t > \frac{F(L)}{\Delta F(L, \Delta L)^2} \times \frac{1}{A_{\mathrm{MOS}}} \times (\mathrm{SD})^2 = \left(\frac{F(L)}{\Delta F(L, \Delta L)}\right)^2 \times \frac{1}{(F(L) \times A_{\mathrm{MOS}})} \times (\mathrm{SD})^2 \tag{6.2}$$

where the first term on the left side is quantified with the knowledge of target's average density length. We formulate equation 2 in two different ways with an inequality, an equality sign and three terms. One can note that the measurement time increases strongly with the decreasing relative flux contrast $F/\Delta F$, which means that it is very important to find a measurement location where this contrast can be as high as possible. The measurement time goes with the square of the Gaussian significance (s.d.) following the basic rules of statistics, that is, the significance can be adjusted for the specific scientific objective: the 'discovery' of an anomaly requires usually 5-sigma (s.d. = 5). The measurement time depends strictly on the square of the significance (s.d.) and therefore can be inferred directly from the 1-sigma value. In this work, we modelled the energy and zenith-angle dependent spectra of muons [75] and integrated these spectra for selected zenith-angles from minimum energies that were derived by simulations of muons through different density lengths of silicon dioxide [76] in the GEANT4 framework [77].

Figure 4 shows the estimated measurement times required to observe given relative density variations with 1 s.d. uncertainty using an observation acceptance of 10 cm^2 sr in case of 500 m (a), 1000 m (b) and 1500 m (c) thick volcano regions with the average density of 1.5 $\mathrm{g\,cm}^{-3}$ (blue lines), 2.1 $\mathrm{g\,cm}^{-3}$ (green lines) and 2.7 $\mathrm{g\,cm}^{-3}$ (red lines) at the zenith-angle of 70° (solid lines), 75° (dashed lines) and 80° (dotted lines), respectively. For example, the measurement time of 3 days is required with an acceptance of 10 cm^2 sr to observe a 20% relative density length increase

[2]See https://arxiv.org/abs/2102.11483v1.

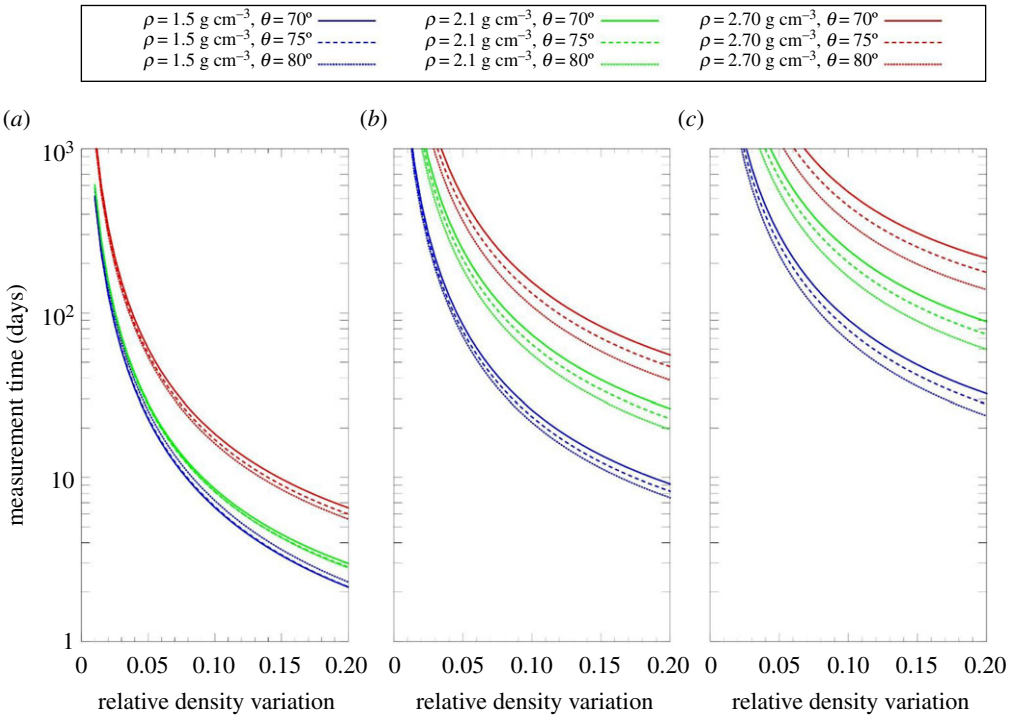

Figure 4. The measurement time is shown for 500 m (*a*), 1000 m (*b*) and 1500 m (*c*) craters with the average densities of 1.5 g cm^{-3} (blue lines), 2.1 g cm^{-3} (green lines) and 2.7 g cm^{-3} (red lines) to observe $\Delta L/L$ relative density length increase with 1 s.d. uncertainty with a detector acceptance of 10 cm^2 sr. (Online version in colour.)

caused by ascending lava across a 500 m thick and crater with the average density of 2.1 g cm^{-3} (see the green curves in figure 4*a*). Using these curves and Equation 6.2, one can estimate the measurement times for different detector acceptances and standard deviations.

Regarding the applicability of muography to volcano monitoring, it is noteworthy that the density difference between rising magma and host rock is not always large. In such a case, we observe the presence of a Neutral Buoyancy Zone (NBZ) where the density of the magma becomes equal to the density of wall rocks [78]. Below a volcanic edifice, the magma ascent is influenced by the given stress field. In some circumstances, neutral buoyancy promotes and controls the formation of sills while suppressing the formation of dikes [79]. Hence, even though magma preferentially spreads at the NBZ level, the NBZ is not a physical barrier for the ascent of the magma [78]. The NBZ can be of significant dimensions if the volatile content dissolved in magma is quite high.

Owing to the complexities explained above, by applying muography, distinguishing rising magma from the host rock can be anything from relatively straightforward to very difficult. However, any rising magma occupies previously observed void space in the conduit. Therefore, it is possible to observe the evolution of magma movement in a dynamic context of the void. The advantage of muography is that it is possible to effectively 'see' inside the volcano and thus observe the movement of magma in real time with a perspective of prediction of volcanic eruptions [80]. By applying muography, Oláh *et al*. [81] imaged the formation of a volcanic plug in the conduit of the Showa Crater of the Sakurajima volcano with a spatial resolution of approximately 60 m. The plug had not been detected earlier by any other geophysical technique. A similar plug has been imaged muographically also at Mt Asama, Japan [82].

After the pioneering work of Nagamine *et al*. [80], muography has been used in multiple applications, archaeology [83,84], including mineral exploration and surveillance of nuclear sites [85–87]. Interestingly, however, the application of muography to volcanology is the one

that shows the best suitability and maturity at the same time [85]. In fact, among the various applications, muography has proved to be particularly effective in the monitoring of volcanic activity, as demonstrated in the research studies carried out at Mt Asama and Sakurajima volcanic centres in Japan [7,39,71,81,88–90], La Soufriere in Guadeloupe [91–96], Mt Vesuvius in Naples [97] and those at Mt Etna [98,99]. Given that the geometry of the muography observation system specifically targets the summit of a volcano and thus makes it possible to oversee the final ascent of magma through its conduit in real time [100], muography detectors can provide useful information during the crucial stages of a volcano prior to an eruptive event as well as on the situation after the eruption. Muography has also been applied to imaging density changes relating to, for example, magma convection [101], magma degassing, the shape of the magma body, empty conduits, hydrothermal activity [102] and major fault lines [103]. Naturally, muography can also be applied for long-term monitoring purposes of dormant volcanoes.

Machine learning (ML) has a potential to automatize and improve the efficiency, reliability and timing of early warnings of volcanic events [104]. However, forecasting with ML of muographic images is currently limited by the moderate number of pixels in the muographic images due to the limited number of collected muon counts. Besides applying high-definition muographic imaging systems, dedicated image processing approaches, e.g. generative adversarial networks [105], can be applied to increase the resolution of muographic images. Thereafter, dedicated tools, e.g. convolutional neural networks (CNN), can efficiently recognize the patterns created by the changes in muon counts due to the density changes inside the volcanic edifice—similar to conventional medical image analysis [106]. Recurrent neural networks) with long–short-term memory [107] are expected to improve the current forecasting performances by 75% [104]. It is worth noting that the forecasting of rarely occurring volcanic eruptions requires the application of anomaly detection algorithms or careful preparation of training data to avoid the overgeneralization and undergeneralization of the applied ML model that would result in fake warnings and poor forecasting capability, respectively. The earlier applied CNN model is processing the muographic images as a black-box function; thus, it was impossible to optimize the prediction conditions. Interpretable and explainable ML has potential to overcome on these limitations and find the hidden precursors of volcanic eruptions [108].

Based on the unique possibilities of muography, this technique complements other existing monitoring techniques used in applied volcanology. In our opinion, one of the major benefits of using muography in volcano monitoring is that it improves the possibilities to reach optimal time scales for our societies to react to early warnings of possible eruptions. Increased understanding about the behavioural pattern of the given volcano is an additional benefit, yet one that is not easy to dismiss either.

7. The experience acquired in the pioneering works on muography applied to volcanoes

The studies of Mt Asama, Honshu, Japan, have shown that the presence of voids and cavities within the premises of a volcano can be successfully detected with muography [90]. Tanaka *et al*. [100] also showed that the average density distribution of the summit area of the Asama volcano provided information on the movement of magma inside the conduit over a month before and a month after the eruption that occurred on 2 February 2009. In this case, the three-dimensional position of the erupted vent was visualized with bidirectional muography. The results showed that the volcano was not axisymmetric [109]. These results indicated that if we assume that the observed density variations are localized in the crater area, uncertainty remains over the shape and alignment of the vent. This uncertainty was constrained with bidirectional computational axial tomography (Mu-CAT). Tanaka *et al*. [109] conducted Mu-CAT to locate a low-density magma pathway found underneath the crater floor in 2006 at Asama volcano, Japan [90]. The shape of the pathway was oval, and its size was determined to be 300 ± 100 m in the W–E direction, and 150 ± 50 m in the N–S direction. Moreover, it was extended toward

the north direction. The reconstructed image was consistent with the direction in which Asama has historically ejected pyroclastic and lava flow. The resolution of the observation was quite good with a margin of error of 10 m over the 700 m of rock, which corresponds to 1.4% error in the path length estimation [100]. The typical angular resolution of 10 milliradians of a muon detector corresponds to the spatial resolution of 10 m at 1 km of distance. The spatial resolution and the density contrast inside the structure can be improved with larger detectors that can detect a larger number of muons within the given period of time. In recent years, the modular muographic observation systems are assembled from typically 3–10 modules and applied in two main measurement arrangements for volcano monitoring: (1) All of the modules are located at a single site, such as at Sakurajima [81] or Mt Vesuvius [97], and oriented towards the summit crater to maximize the sensitive surface up to a few square metres and minimize the observation time from a few months to a few weeks. (2) Multiple modules are installed at different sites around the volcanic edifice, e.g. at La Soufriere volcano [91,93,94], to integrate muography with absolute gravimetry or seismic monitoring. The field experiences with the transportation, installation and long-term operation of different types of tracking detectors suggested optimizing the design with a typical module surface area of approximately 1 m^2 and a weight of a few tens of kilograms independently from the applied technology. This is particularly valuable when observing summits of active volcanoes that pose particularly high hazard risks or are difficult to access to deploy other types of instruments [90].

In the study of Tanaka *et al.* [82], the density of the lava mound (2.76–2.84 g cm^{-3}) was distinguished from the density of the surrounding rocks (2.27–2.33 g cm^{-3}). These density values are typical to andesitic lava and also agree with the density values of the surrounding rocks—andesitic explosive products of the eruption of 1783—that range from 1.40 to 2.68 g cm^{-3} [110]. Tanaka *et al*. [100] applied muography to estimate the mass loss inside the Asama crater due to the eruption of 2 February 2009. According to their analysis, the muography data revealed that this particular eruption led to a mean volume of erupted ash and other volcanic ejecta of a total of 65 250 tons (with a confidence level of 1σ). The given mass loss measured by muography was consistent with the amount estimated from volcanic ash studies.

Furthermore, the densely distributed traffic tunnels in Japan allowed comparing the bulk sedimentary and volcanic rock densities acquired with muographic and gravimetric techniques. As a general trend, it was noticed that the densities tend to be higher for older rock than those of younger rocks [111]. Importantly, density values estimated from muographic data are consistent with those interpreted from gravimetric data. Tanaka [111] also measured the bulk density of the volcanic peninsula (Izu Peninsula, Japan) and compared the results with those of the laboratory-based measurements. Consequently, it was found that the peninsula is porous with multi-cracks such as seismic faults that reflect its tectonic history.

Regarding the reliability of muographically derived estimates of average density, the study of Tanaka [111] is also interesting. The density measurements made muographically at the Unzen volcano, Japan [39], are consistent with the density measurements conducted in the same area by applying the Archimedean principle on dry rock samples using a mobile field-based density measurement tool [112]. The density of solid lava calculated from muography data (approx. 2.0 g cm^{-3}) is close to the mean density of 2.1 g cm^{-3} reported by Kueppers *et al*. [112] from Unzen, even though the whole range of densities was as broad as 1.6–2.4 g cm^{-3}.

8. The recent experience acquired at volcanic centres by applying muography to volcanoes

One of the disadvantages of the muography method is that the muographically acquired densities are averaged along with the observed muon trajectories (i.e. individually for each line of observation). In this respect, muography 'collects' information over much larger volumes of rock than hand-picked rock samples [91]. In fact, it is definitely an advantage for geologists who typically have no other means to study non-exposed rocks than drilling or deploying

other (seismic or electric) geophysical arrays. Nevertheless, many studies demonstrate how muography is indeed a very valuable tool in applied volcanology if it is applied correctly, and the drawbacks of this particular method are kept in mind while interpreting the recorded data. The said drawbacks include the above disadvantage and the relatively long deployment time required for recording a statistically satisfactory amount of data (i.e. muon passings). As an example concerning the value of muography in applied volcanology, the experiments carried out at La Soufrière in the Lesser Antilles Volcanic Arc, Guadeloupe, Caribbean, have revealed that contrasted densities in the local volcanic rocks may be partly explained with the presence of voids inside the volcanic structure [91]. Another example, the muographic data acquired at Mt Etna has revealed a set of large fractures and cavities resulting from the collapse of the upper structure of the Northeast Crater due to internal erosion by gases at high temperature [99]. This study focused on the volcano-tectonic evolution of the volcano and its results are a significant advancement over the previous experiments on muography in Mt Etna, such as that of Lo Presti *et al*. [98]. The latter, earlier work focused on the design and testing of the muon detection instruments in an extinct volcanic cone (Monti Rossi) of Mt Etna.

Data acquired at Unzen lava dome, Japan, show that it is possible to obtain a detailed image of the structure of the growing high-density material (the core) within the low-density brecciated material, assuming one just continues measurements long enough [39]. Usage of muography for such purposes can also be useful for monitoring such eventual phenomena as dome collapses, as has already been conducted, for example, in Soufrière Hills in Montserrat, Caribbean [39,113]. Moreover, the data acquired at Sakurajima Kyushu, Japan, from 2 February to 1 June 2018 show how the magma movement inside the conduit can be monitored with time [7,71,81,89,104,114]. Figure 5 shows the average density increase in the summit area of Sakurajima during the eruption. This observation shows the magma ascent and probably subsequent descent in the lateral conduit leading to the crater Showa. The speed of the ascent and descent of magma was much faster than that observed in the Satsuma-Iwojima volcano in Kyushu, Japan, when it erupted in 2013, indicating the difference in magma viscosity [89]. The amount of the magma ascent tends to increase as the eruption intervals become longer. The difference between (*a*), (*b*), (*c*) and (*d*) are eruption intervals of (*a*) 0–2 h, (*b*) 2–5 h, (*c*) 5–10 h and (*d*) greater than or equal to10 h.

Figure 6 shows a quantitative expression near the active crater Showa. The region is divided into 12 areas (figure 6*a*). The time-sequential plot corresponding to each area is shown in figure 6*b*. The time zero in the horizontal axis corresponds to the moment when the eruption started. As shown in G and H of figure 6*b*, the reduction in the muon flux due to the magma ascent right before and after the eruption is quite evident with the outlier point plotting well away from the main line. The passage of magma affects the muon count due to its higher density compared to the surrounding rocks. It takes a while (approx. 30 min) for the ascending magma to fill the inter-particle spaces inside the brecciated (and porous) material remaining from previous eruptions located right underneath the crater floor. Once magma saturates this material, it pours over the crater floor. After the eruption, it takes a while to drain the remaining magma from the porous material (again approx. 30 min) and draw it back to the deeper regions in the crater-magma chamber system. Another interesting phenomenon shown in figure 7 is the muon reduction rate r in hours, which we interpret to be related to a different eruption interval. We explain this phenomenon with a more detailed example in figure 6. In figures 5 and 6, the muon-counting rates are data points associated with error bars. The horizontal axis shows the eruption intervals, as shown in H of figure 6*b*. The ordinary rate N_{ord} is the muon-counting rate recorded when the volcano did not erupt. It was expected that the muon-counting rate during the eruption would have been lower when the eruption occurred. However, if the eruption interval is short, less magma ascends in the unit of time. As the eruption interval increases, the amount of magma ascent also increases in the unit of time.

As yet another example of recent muography research on volcanoes, between 2014 and 2016, Nomura *et al*. [104] applied the deep learning technique to muographic data acquired at Sakurajima volcano, Japan and eruption prediction was attempted based on the seven consecutive daily generated muograms prior to the prediction day. As a consequence, the prediction accuracy

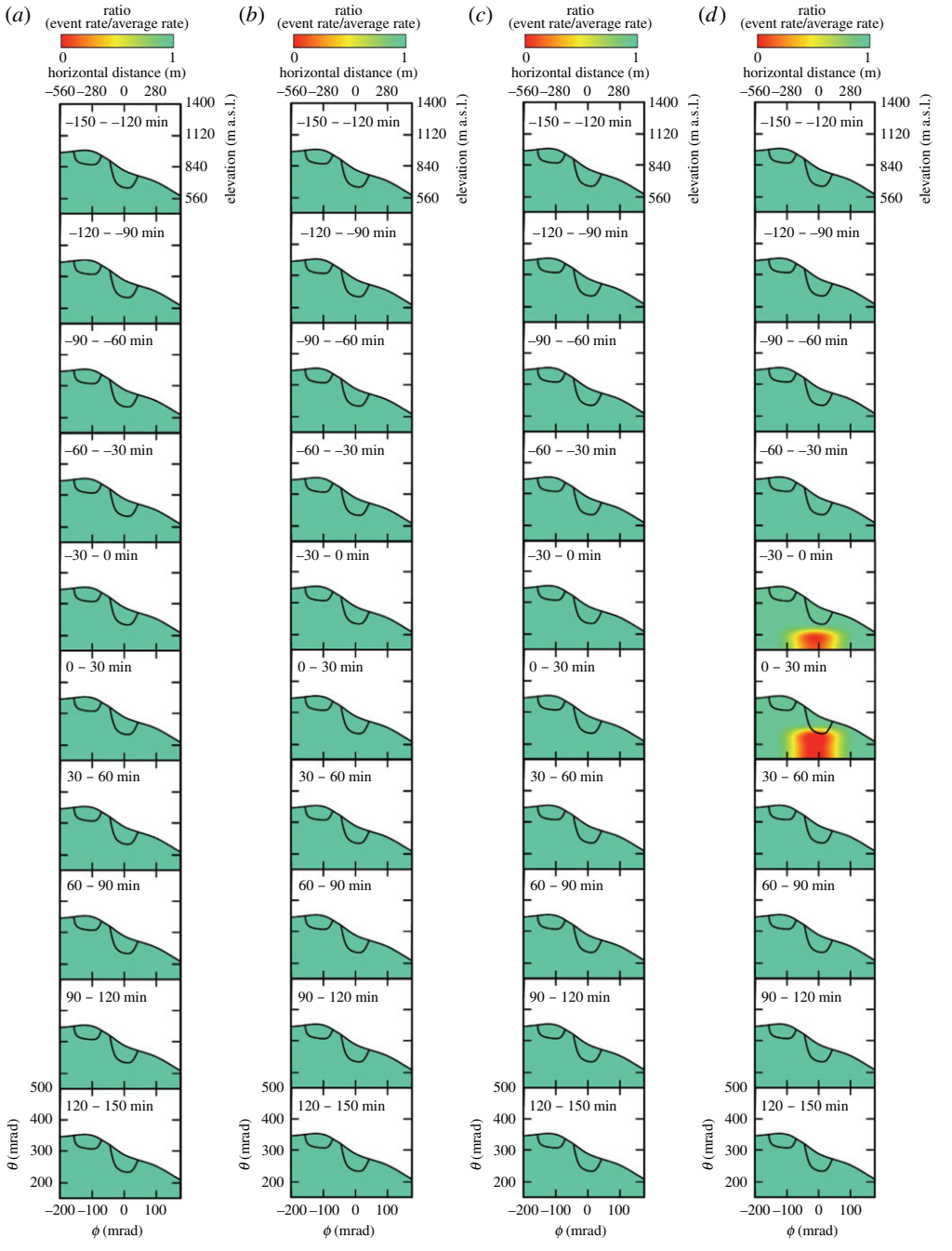

Figure 5. Time-sequential muographic maps as measured near the most active crater of the Sakurajima volcano, Japan (Showa Crater), shown for different eruption intervals of (*a*) 0–2 h, (*b*) 2–5 h, (*c*) 5–10 h and (*d*) ≥10 h. The variations with a statistical confidence level of more than 99% are plotted [114]. Each data point was calculated by averaging over 30 muograms. (Online version in colour.)

was better than 70%. The extensive eruption episode at Showa Crater ended in 2017, and a new episode started at another crater. In the time-sequential muographic images captured between 2017 and 2018, a volcanic plug was generated underneath Showa Crater in accordance with this change in the eruption sequence [81].

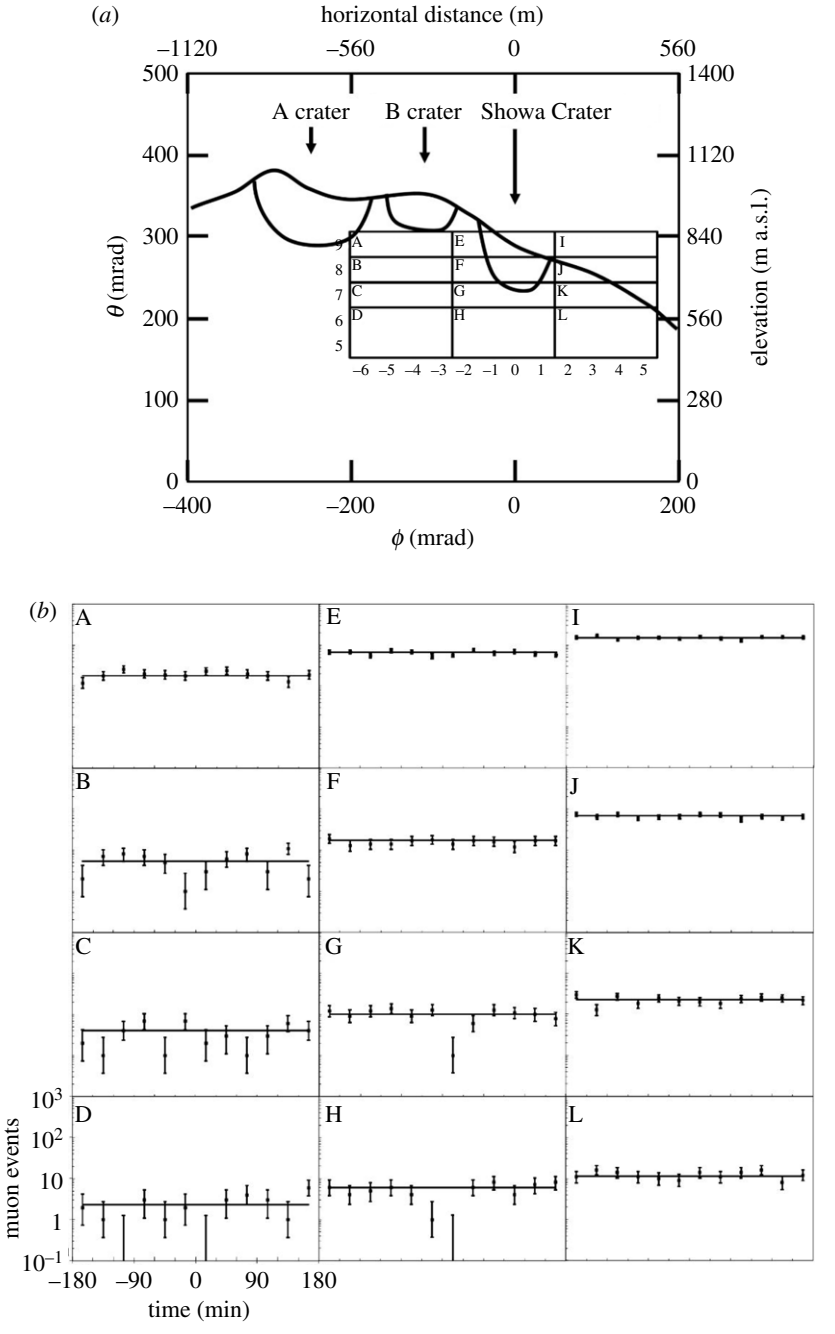

Figure 6. Cross-sectional view of Sakurajima volcano, Japan, including Minamidake (A and B) and Showa craters (*a*), and comparison of the time-sequential muon events for different regions near the active craters (*b*). The grids labelled with the letters from A to L in (*a*) correspond to those in the (*b*) [114]. Each data point was calculated by averaging over 30 muograms. The distance of the detector from the volcano is about 500 m (e.g. [82]).

9. Conclusion

We have shown how muography can achieve a good resolution for monitoring the latest stage of volcanic activity and how it can be applied to acquire information on the evolution of a volcano in real time. In brief, muography is a simple method with a capability to contribute to

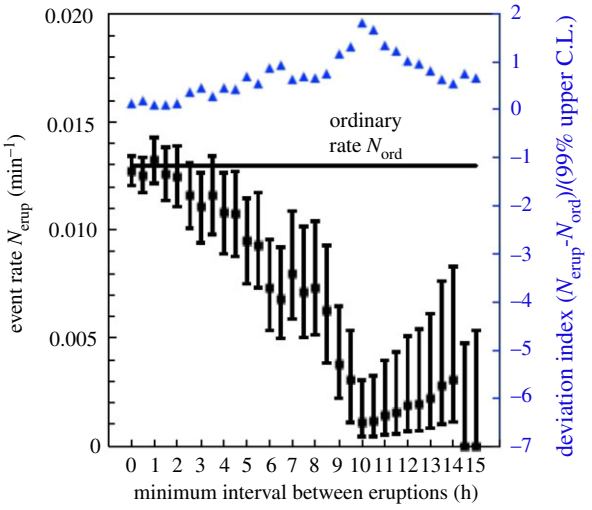

Figure 7. Connection between the muon rate right after eruptions and the time interval between eruptions. The averaged muon rate is also shown. The error bars indicate the upper and lower 99% confidence level limits. Triangular symbols indicate the deviation index defined in the main text [114]. (Online version in colour.)

applied volcanology with the dynamic observations of magma in conduit, magma degassing, eruption dynamics and volcanic hazards following their evolutions over time. We have also shown how the averaged density over a thick volcanic structure is perfectly consistent with punctual measurements obtained by other methods. Obviously, using muography does not mean replacing other well-established methods of monitoring that have proven useful but integrate them with additional information. Recently, it was also shown how muography offers a remotely operable technique to monitor thickness variations in tephra fallouts [40,115]. This indicates that muography has the potential to improve the predictability of lahars. It is also worth pointing out that a single MuTe used only in a single location can only partially map the density of a volcano unless it is a relatively small body, or the telescope is located far away (and then the price is paid in angular resolution). If high-level angular precision is needed, muography must be carried out in multiple locations so that the separate partial volumes of the target, each imaged with muographic means from individual observation locations, can be tomographically combined. The different tracking systems operate independently and maximize the robustness of the muography observation system against the malfunctioning of detector elements or extreme weather events. Detector control, data acquisition are allowed by a local network that is accessible from remote places. This arrangement provides automated data management and analysis that allows to realize real-time muography by increasing the number of modules [84,116]. The design of the recently applied systems is expected to be applicable in future large-sized systems, such as the multi-aspect-geo-muography-array (MAGMA) experiment[3], which is designed to operate with a few hundreds of modules to reach the desired time imaging time of a few hours for early warning.

By combining all the existing methods, including muography, researchers have more tools to make significant advancements in volcanic hazard monitoring. Essentially, the capabilities of muography are particularly useful during the final moments of the first (alert) phase onwards to the first stages of volcanic unrest, corresponding to the time when the danger to the surrounding population increases and prompts decisions about rapid but ordinate evacuation must be made; during this decision, there must be a balance between the need to protect the lives of the citizens and the need to protect the economic health of the community. Therefore, providing

[3]See https://pdfs.semanticscholar.org/3c85/b7b07f4f915d935d5f198b28ce0e9b09fad8.pdf.

multiparameter data would aid in such decision-making process. Furthermore, muography may also be used to monitor volcanoes on a longer term basis, perhaps as an integral part of multiparameter monitoring systems combining continuous seismic, ground deformation, gas emission, thermal monitoring and muography data. Suppose muography is not applied by permanent muography stations, but the detectors are transported to the site when needed. In that case, data from all the other methods of volcanic monitoring can be used as a basis to evaluate and finally decide when the first phase is close to its end so that muography can take place.

Ethics. Not applicable.

Data accessibility. Data will be made available upon request.

Authors' contributions. G.L., H.K.M.T., D.V., L.O., M.H., P.K. and D.L.P. conceived, designed the study and drafted the manuscript. H.K.M.T. performed data analysis and prepared the figures with L.O. C.M, C.F., G.B., K.S., L.T., S.S. and J.J. partially drafted and reviewed the manuscript. All authors read and approved the manuscript.

Competing interests. The author(s) declare that they have no competing interests.

Funding. Nothing to report.

Acknowledgements. The authors thank the editor Chris Garrett and three anonymous reviewers who significantly improved the original manuscript with their comments. Many thanks to Gene Walter Schmidt for the modification and improvement of figure 7. M. Holma wishes to acknowledge that from the point of view of Arctic Planetary Science Institute, which is one of his affiliations, this paper is the APSI Contribution #17.

References

1. Antoni T *et al.* 2001 Electron, muon, and hadron lateral distributions measured in air showers by the KASCADE experiment. *Astropart. Phys.* **14**, 245–260. (doi:10.1016/S0927-6505(00)00125-0)
2. Cazon L, Conceição R, Pimenta M, Santos E. 2012 A model for the transport of muons in extensive air showers. *Astropart. Phys.* **36**, 211–223. (doi:10.1016/j.astropartphys.2012.05.017)
3. Hörandel JR. 2008 The origin of galactic cosmic rays. *Nucl. Instrum. Methods Phys. Res. Sect. A* **588**, 181–188. (doi:10.1016/j.nima.2008.01.036)
4. Bonechi L, D'Alessandro R, Giammanco A. 2020 Atmospheric muons as an imaging tool. *Rev. Phys.* **5**, 100038. (doi:10.1016/j.revip.2020.100038)
5. Aad G *et al.* 2019 Search for electroweak diboson production in association with a high-mass dijet system in semileptonic final states in pp collisions at s = 13 TeV with the ATLAS detector. *Phys. Rev. D* **100**, 32007. (doi:10.1103/PhysRevD.100.032007)
6. Aad G *et al.* 2016 Muon reconstruction performance of the ATLAS detector in proton–proton collision data at s = 13 TeV. *Eur. Phys. J. C* **76**, 1–30. (doi:10.1140/epjc/s10052-016-4120-y)
7. Oláh L, Tanaka HKM, Ohminato T, Varga D. 2018 High-definition and low-noise muography of the Sakurajima volcano with gaseous tracking detectors. *Sci. Rep.* **8**, 3207. (doi:10.1038/s41598-018-21423-9)
8. Tanaka HKM. 2013 Subsurface density mapping of the earth with cosmic ray muons. *Nucl. Phys. B Proc. Suppl.* **243–244**, 239–248. (doi:10.1016/j.nuclphysbps.2013.09.020)
9. Scarpa R, Tilling RI, Chouet BA. 1996 New methods and future trends in seismological volcano monitoring. In *Monitoring and mitigation of volcano hazards*, pp. 23–97. Berlin, Germany: Springer.
10. Magee C *et al.* 2016 Lateral magma flow in mafic sill complexes. *Geosphere* **12**, 809–841. (doi:10.1130/GES01256.1)
11. Smets B *et al.* 2014 Detailed multidisciplinary monitoring reveals pre- and co-eruptive signals at Nyamulagira volcano (North Kivu, Democratic Republic of Congo). *Bull. Volcanol.* **76**, 1–35. (doi:10.1007/s00445-013-0787-1)
12. McCormick BT, Herzog M, Yang J, Edmonds M, Mather TA, Carn SA, Hidalgo S, Langmann B. 2014 A comparison of satellite- and ground-based measurements of SO_2 emissions from Tungurahua volcano, Ecuador. *J. Geophys. Res.* **119**, 4264–4285. (doi:10.1002/2013JD019771)
13. Karagulian F, Clarisse L, Clerbaux C, Prata AJ, Hurtmans D, Coheur PF. 2010 Detection of volcanic SO_2, ash, and H_2SO_4 using the Infrared Atmospheric Sounding Interferometer (IASI). *J. Geophys. Res.* **115**, D00L02. (doi:10.1029/2009JD012786)

14. Corradini S, Merucci L, Prata AJ, Piscini A. 2010 Volcanic ash and SO_2 in the 2008 Kasatochi eruption: retrievals comparison from different IR satellite sensors. *J. Geophys. Res.* **115**, D00L21. (doi:10.1029/2009JD013634)
15. Rix M *et al.* 2012 Volcanic SO_2, BrO and plume height estimations using GOME-2 satellite measurements during the eruption of Eyjafjallajökull in May 2010. *J. Geophys. Res.* **117**, 0–19. (doi:10.1029/2011JD016718)
16. Carn SA, Fioletov VE, Mclinden CA, Li C, Krotkov NA. 2017 A decade of global volcanic SO2 emissions measured from space. *Sci. Rep.* **7**, 1–12. (doi:10.1038/srep44095)
17. Johnson JB, Palma JL. 2015 Lahar infrasound associated with Volcán Villarrica's 3 March 2015 eruption. *Geophys. Res. Lett.* **42**, 6324–6331. (doi:10.1002/2015GL065024)
18. Iannaccone G, Guardato S, Vassallo M, Elia L, Beranzoli L. 2009 A new multidisciplinary marine monitoring system for the surveillance of volcanic and seismic areas. *Seismol. Res. Lett.* **80**, 203–213. (doi:10.1785/gssrl.80.2.203)
19. Monna S *et al.* 2014 Underwater geophysical monitoring for European Multidisciplinary Seafloor and water column Observatories. *J. Mar. Sys.* **130**, 12–30. (doi:10.1016/j.jmarsys.2013.09.010)
20. Fox CG, Chadwick WW, Embley RW. 2001 Direct observation of a submarine volcanic eruption from a sea-floor instrument caught in a lava flow. *Nature* **412**, 727–729. (doi:10.1038/35089066)
21. Chadwick WW, Nooner SL, Butterfield DA, Lilley MD. 2012 Seafloor deformation and forecasts of the April 2011 eruption at Axial Seamount. *Nat. Geosci.* **5**, 474–477. (doi:10.1038/ngeo1464)
22. Ballu V *et al.* 2009 A seafloor experiment to monitor vertical deformation at the Lucky Strike volcano, Mid-Atlantic Ridge. *J. Geod.* **83**, 147–159. (doi:10.1007/s00190-008-0248-3)
23. Andronico D, Corsaro RA, Cristaldi A, Polacci M. 2008 Characterizing high energy explosive eruptions at Stromboli volcano using multidisciplinary data: an example from the 9 January 2005 explosion. *J. Volcanol. Geotherm. Res.* **176**, 541–550. (doi:10.1016/j.jvolgeores.2008.05.011)
24. Spampinato L, Calvari S, Oppenheimer C, Boschi E. 2011 Volcano surveillance using infrared cameras. *Earth Sci. Rev.* **106**, 63–91. (doi:10.1016/j.earscirev.2011.01.003)
25. Poulidis AP, Takemi T, Shimizu A, Iguchi M, Jenkins SF. 2018 Statistical analysis of dispersal and deposition patterns of volcanic emissions from Mt. Sakurajima, Japan. *Atmos. Environ.* **179**, 305–320. (doi:10.1016/j.atmosenv.2018.02.021)
26. Leibrandt S, Le Pennec JL. 2015 Towards fast and routine analyses of volcanic ash morphometry for eruption surveillance applications. *J. Volcanol. Geotherm. Res.* **297**, 11–27. (doi:10.1016/j.jvolgeores.2015.03.014)
27. Nurfiani D, Bouvet de Maisonneuve C. 2018 Furthering the investigation of eruption styles through quantitative shape analyses of volcanic ash particles. *J. Volcanol. Geotherm. Res.* **354**, 102–114. (doi:10.1016/j.jvolgeores.2017.12.001)
28. Bonaccorso A, Bonforte A, Calvari S, Del Negro C, Di Grazia G, Ganci G, Neri M, Vicari A, Boschi E. 2011 The initial phases of the 2008-2009 Mount Etna eruption: a multidisciplinary approach for hazard assessment. *J. Geophys. Res.* **116**, B03203. (doi:10.1029/2010JB007906)
29. Geirsson H *et al.* 2014 Multidisciplinary observations of the 2011 explosive eruption of Telica volcano, Nicaragua: implications for the dynamics of low-explosivity ash eruptions. *J. Volcanol. Geotherm. Res.* **271**, 55–69. (doi:10.1016/j.jvolgeores.2013.11.009)
30. Rasmussen DJ, Plank TA, Roman DC, Power JA, Bodnar RJ, Hauri EH. 2018 When does eruption run-up begin? Multidisciplinary insight from the 1999 eruption of Shishaldin volcano. *Earth Planet. Sci. Lett.* **486**, 1–14. (doi:10.1016/j.epsl.2018.01.001)
31. Scollo S, Prestifilippo M, Spata G, D'Agostino M, Coltelli M. 2009 Monitoring and forecasting Etna volcanic plumes. *Nat. Hazards Earth Syst. Sci.* **9**, 1573–1585. (doi:10.5194/nhess-9-1573-2009)
32. Pistolesi M, Delle Donne D, Pioli L, Rosi M, Ripepe M. 2011 The 15 March 2007 explosive crisis at Stromboli volcano, Italy: assessing physical parameters through a multidisciplinary approach. *J. Geophys. Res.* **116**, B12206. (doi:10.1029/2011JB008527)
33. Scharff L, Hort M, Harris AJL, Ripepe M, Lees JM, Seyfried R. 2008 Eruption dynamics of the SW crater of Stromboli volcano, Italy — an interdisciplinary approach. *J. Volcanol. Geotherm. Res.* **176**, 565–570. (doi:10.1016/j.jvolgeores.2008.05.008)
34. Johnson JB, Ripepe M. 2011 Volcano infrasound: a review. *J. Volcanol. Geotherm. Res.* **206**, 61–69. (doi:10.1016/j.jvolgeores.2011.06.006)

35. Takahashi T. 2004 ISRM suggested methods for land geophysics in rock engineering. *Int. J. Rock Mech. Min. Sci.* **41**, 885–914. (doi:10.1016/j.ijrmms.2004.02.009)
36. Ulivieri G, Ripepe M, Marchetti E. 2013 Infrasound reveals transition to oscillatory discharge regime during lava fountaining: implication for early warning. *Geophys. Res. Lett.* **40**, 3008–3013. (doi:10.1002/grl.50592)
37. Cannavò F, Camacho AG, González PJ, Mattia M, Puglisi G, Fernández J. 2015 Real time tracking of magmatic intrusions by means of ground deformation modeling during volcanic crises. *Sci. Rep.* **5**, 10 970–10 979. (doi:10.1038/srep10970)
38. Kilburn CRJ, Sammonds PR. 2005 Maximum warning times for imminent volcanic eruptions. *Geophys. Res. Lett.* **32**, L24313. (doi:10.1029/2005GL024184)
39. Tanaka HKM. 2016 Instant snapshot of the internal structure of Unzen lava dome, Japan with airborne muography. *Sci. Rep.* **6**, 39741. (doi:10.1038/srep39741)
40. Oláh L, Tanaka HKM, Hamar G. 2021 Muographic monitoring of hydrogeomorphic changes induced by post-eruptive lahars and erosion of Sakurajima volcano. *Sci. Rep.* **11**, 1–12. (doi:10.1038/s41598-021-96947-8)
41. De la Cruz-Reyna S, Tilling RI. 2008 Scientific and public responses to the ongoing volcanic crisis at Popocatépetl Volcano, Mexico: importance of an effective hazards-warning system. *J. Volcanol. Geotherm. Res.* **170**, 121–134. (doi:10.1016/j.jvolgeores.2007.09.002)
42. Leonard GS *et al.* 2014 Integrating multidisciplinary science, modelling and impact data into evolving, syn-event volcanic hazard mapping and communication: a case study from the 2012 Tongariro eruption crisis, New Zealand. *J. Volcanol. Geotherm. Res.* **286**, 208–232. (doi:10.1016/j.jvolgeores.2014.08.018)
43. Marzocchi W, Newhall C, Woo G. 2012 The scientific management of volcanic crises. *J. Volcanol. Geotherm. Res.* **247–248**, 181–189. (doi:10.1016/j.jvolgeores.2012.08.016)
44. Mei ETW, Lavigne F, Picquout A, de Bélizal E, Brunstein D, Grancher D, Sartohadi J, Cholik N, Vidal C. 2013 Lessons learned from the 2010 evacuations at Merapi volcano. *J. Volcanol. Geotherm. Res.* **261**, 348–365. (doi:10.1016/j.jvolgeores.2013.03.010)
45. Leone F, Gaillard JC. 1999 Analysis of the institutional and social responses to the eruption and the lahars of Mount Pinatubo volcano from 1991 to 1998 (Central Luzon, Philippines). *GeoJournal* **49**, 223–238. (doi:10.1023/A:1007076704752)
46. Hincks TK, Komorowski JC, Sparks SR, Aspinall WP. 2014 Retrospective analysis of uncertain eruption precursors at La Soufrière volcano, Guadeloupe, 1975–77: volcanic hazard assessment using a Bayesian Belief Network approach. *J. Appl. Volcanol.* **3**, 1–26. (doi:10.1186/2191-5040-3-3)
47. Sparks R, Aspinall W, Crosweller H, Hincks T. 2013 *Risk and uncertainty assessment for natural hazards*, 1st edn. Cambridge, UK: Cambridge University Press. See https://books.google.cl/books?id=fHEhAwAAQBAJ&printsec=frontcover&hl=it#v=onepage&q&f=false.
48. Rolandi G. 2010 Volcanic hazard at Vesuvius: an analysis for the revision of the current emergency plan. *J. Volcanol. Geotherm. Res.* **189**, 347–362. (doi:10.1016/j.jvolgeores.2009.08.007)
49. Siebert L, Cottrell E, Venzke E, Andrews B. 2015 Earth's volcanoes and their eruptions: an overview. In *The encyclopedia of volcanoes*. Amsterdam, The Netherlands: Elsevier.
50. Tilling RI. 1989 Volcanic hazards and their mitigation: progress and problems. *Rev. Geophys.* **27**, 237. (doi:10.1029/RG027i002p00237)
51. Scarpa R, Tilling RI, McNutt SR. 1996 Seismic monitoring and eruption forecasting of volcanoes: a review of the state-of-the-art and case histories. In *Monitoring and mitigation of volcano hazards*, pp. 99–146. Berlin, Germany: Springer.
52. Woo G. 2008 Probabilistic criteria for volcano evacuation decisions. *Nat. Hazards* **45**, 87–97. (doi:10.1007/s11069-007-9171-9)
53. Gaillard JC. 2008 Alternative paradigms of volcanic risk perception: the case of Mt. Pinatubo in the Philippines. *J. Volcanol. Geotherm. Res.* **172**, 315–328. (doi:10.1016/j.jvolgeores.2007.12.036)
54. Guffanti M, Mayberry GC, Casadevall TJ, Wunderman R. 2009 Volcanic hazards to airports. *Nat. Hazards* **51**, 287–302. (doi:10.1007/s11069-008-9254-2)
55. Budd L, Griggs S, Howarth D, Ison S. 2011 A fiasco of volcanic proportions? eyjafjallajökull and the closure of European airspace. *Mobilities* **6**, 31–40. (doi:10.1080/17450101.2011.532650)
56. Annen C, Wagner J-J. 2003 The impact of volcanic eruptions during the 1990s. *Nat. Hazards Rev.* **4**, 169–175. (doi:10.1061/(ASCE)1527-6988(2003)4:4(169))

57. Folch A, Sulpizio R. 2010 Evaluating long-range volcanic ash hazard using supercomputing facilities: application to Somma-Vesuvius (Italy), and consequences for civil aviation over the Central Mediterranean Area. *Bull. Volcanol.* **72**, 1039–1059. (doi:10.1007/s00445-010-0386-3)
58. Wilson TM, Stewart C, Sword-Daniels V, Leonard GS, Johnston DM, Cole JW, Wardman J, Wilson G, Barnard ST. 2012 Volcanic ash impacts on critical infrastructure. *Phys. Chem. Earth Parts A/B/C* **45–46**, 5–23. (doi:10.1016/j.pce.2011.06.006)
59. Picquout A, Lavigne F, Mei ETW, Grancher D, Noer C, Vidal CM, Hadmoko DS. 2013 Air traffic disturbance due to the 2010 Merapi volcano eruption. *J. Volcanol. Geotherm. Res.* **261**, 366–375. (doi:10.1016/j.jvolgeores.2013.04.005)
60. Alexander D. 2013 Volcanic ash in the atmosphere and risks for civil aviation: a study in European crisis management. *Int. J. Disaster Risk Sci.* **4**, 9–19. (doi:10.1007/s13753-013-0003-0)
61. Sulpizio R, Folch A, Costa A, Scaini C, Dellino P. 2012 Hazard assessment of far-range volcanic ash dispersal from a violent Strombolian eruption at Somma-Vesuvius volcano, Naples, Italy: implications on civil aviation. *Bull. Volcanol.* **74**, 2205–2218. (doi:10.1007/s00445-012-0656-3)
62. Thouret JC. 1999 Urban hazards and risks; consequences of earthquakes and volcanic eruptions: an introduction. **49**, 131–135. (doi:10.2307/41147408)
63. Simpson A, Johnson RW, Cummins P. 2011 Volcanic threat in developing countries of the Asia-Pacific region: probabilistic hazard assessment, population risks, and information gaps. *Nat. Hazards* **57**, 151–165. (doi:10.1007/s11069-010-9601-y)
64. Jenkins SF, Spence RJS, Fonseca JFBD, Solidum RU, Wilson TM. 2014 Volcanic risk assessment: quantifying physical vulnerability in the built environment. *J. Volcanol. Geotherm. Res.* **276**, 105–120. (doi:10.1016/j.jvolgeores.2014.03.002)
65. Biass S, Frischknecht C, Bonadonna C. 2012 A fast GIS-based risk assessment for tephra fallout: the example of Cotopaxi volcano, Ecuador-Part II: vulnerability and risk assessment. *Nat. Hazards* **64**, 615–639. (doi:10.1007/s11069-012-0270-x)
66. Barclay J *et al.* 2008 Framing volcanic risk communication within disaster risk reduction: finding ways for the social and physical sciences to work together. *Geol. Soc. Lond. Spec. Publ.* **305**, 163–177. (doi:10.1144/SP305.14)
67. Schmidtlein MC, Deutsch RC, Piegorsch WW, Cutter SL. 2008 A sensitivity analysis of the social vulnerability index. *Risk Anal.* **28**, 1099–1114. (doi:10.1111/j.1539-6924.2008.01072.x)
68. Pearson L, Pelling M. 2015 The UN Sendai framework for disaster risk reduction 2015–2030: negotiation process and prospects for science and practice. *J. Extreme Events* **02**, 1571001. (doi:10.1142/S2345737615710013)
69. Fournier D'Albe EM. 1979 Objectives of volcanic monitoring and prediction. *J. Geol. Soc.* **136**, 321–326. (doi:10.1144/gsjgs.136.3.0321)
70. Mitra SM, Sarkar PK, Kudryavtsev VA. 2009 Empirical expressions for angular deviation of muons transmitted through slabs of iron, lead and uranium. *Nucl. Instrum. Methods Phys. Res. Sect. A* **604**, 684–693. (doi:10.1016/j.nima.2009.02.037)
71. Oláh L, Tanaka HKM, Hamar G, Varga D. 2019 Investigation of the limits of high-definition muography for observation of Mt Sakurajima. *Phil. Trans. R. Soc. A* **377**, 20180135. (doi:10.1098/rsta.2018.0135)
72. Oláh L, Varga D. 2017 Investigation of soft component in cosmic ray detection. *Astropart. Phys.* **93**, 17–27. (doi:10.1016/j.astropartphys.2017.06.002)
73. Nishiyama R, Taketa A, Miyamoto S, Kasahara K. 2016 Monte Carlo simulation for background study of geophysical inspection with cosmic-ray muons. *Geophys. J. Int.* **206**, 1039–1050. (doi:10.1093/gji/ggw191)
74. Lesparre N, Gibert D, Marteau J, Déclais Y, Carbone D, Galichet E. 2010 Geophysical Muon imaging: feasibility and limits. *Geophys. J. Int.* **183**, 1348–1361. (doi:10.1111/j.1365-246X.2010.04790.x)
75. Guan M, Chu MC, Cao J, Luk KB, Yang C. 2015 A parametrization of the cosmic-ray muon flux at sea-level. (https://arxiv.org/abs/1509.06176)
76. Groom DE, Mokhov N V, Striganov SI. 2001 Muon stopping power and range tables 10 MeV–100 TeV. *At. Data Nucl. Data Tables* **78**, 183–356. (doi:10.1006/adnd.2001.0861)
77. Agostinelli S *et al.* 2003 Geant4—a simulation toolkit. *Nucl. Instrum. Methods Phys. Res. Sect. A* **506**, 250–303. (doi:10.1016/S0168-9002(03)01368-8)
78. Rivalta E, Taisne B, Bunger AP, Katz RF. 2015 A review of mechanical models of dike propagation: schools of thought, results and future directions. *Tectonophysics* **638**, 1–42. (doi:10.1016/j.tecto.2014.10.003)

79. Menand T. 2011 Physical controls and depth of emplacement of igneous bodies: a review. *Tectonophysics* **500**, 11–19. (doi:10.1016/j.tecto.2009.10.016)
80. Nagamine K, Iwasaki M, Shimomura K, Ishida K. 1995 Method of probing inner-structure of geophysical substance with the horizontal cosmic-ray muons and possible application to volcanic eruption prediction. *Nucl. Instrum. Methods Phys. Res. Sect. A* **356**, 585–595. (doi:10.1016/0168-9002(94)01169-9)
81. Oláh L, Tanaka HKM, Ohminato T, Hamar G, Varga D. 2019 Plug formation imaged beneath the active craters of Sakurajima Volcano with muography. *Geophys. Res. Lett.* **46**, 10 417–10 424. (doi:10.1029/2019gl084784)
82. Tanaka HKM, Nakano T, Takahashi S, Yoshida J, Ohshima H, Maekawa T, Watanabe H, Niwa K. 2007 Imaging the conduit size of the dome with cosmic-ray muons: the structure beneath Showa-Shinzan Lava Dome, Japan. *Geophys. Res. Lett.* **34**, L22311. (doi:10.1029/2007GL031389)
83. Morishima K *et al.* 2017 Discovery of a big void in Khufu's Pyramid by observation of cosmic-ray muons. *Nature* **552**, 386–390. (doi:10.1038/nature24647)
84. Procureur S, Attié D. 2019 Development of high-definition muon telescopes and muography of the Great Pyramid. *C.R. Phys.* **20**, 521–528. (doi:10.1016/j.crhy.2019.09.003)
85. Kaiser R. 2019 Muography: overview and future directions. *Phil. Trans. R. Soc. A* **377**, 20180049. (doi:10.1098/rsta.2018.0049)
86. Schouten D, Ledru P. 2018 Muon tomography applied to a dense uranium deposit at the McArthur River mine. *J. Geophys. Res.* **123**, 8637–8652. (doi:10.1029/2018JB015626)
87. Perry J *et al.* 2013 Imaging a nuclear reactor using cosmic ray muons. *J. Appl. Phys.* **113**, 184909. (doi:10.1063/1.4804660)
88. Tanaka HKM, Uchida T, Tanaka M, Shinohara H, Taira H. 2009 Cosmic-ray muon imaging of magma in a conduit: degassing process of Satsuma-Iwojima Volcano, Japan. *Geophys. Res. Lett.* **36**, L01304. (doi:10.1029/2008GL036451)
89. Tanaka HKM, Kusagaya T, Shinohara H. 2014 Radiographic visualization of magma dynamics in an erupting volcano. *Nat. Commun.* **5**, 3381. (doi:10.1038/ncomms4381)
90. Tanaka HKM *et al.* 2007 High resolution imaging in the inhomogeneous crust with cosmic-ray muon radiography: the density structure below the volcanic crater floor of Mt. Asama, Japan. *Earth Planet. Sci. Lett.* **263**, 104–113. (doi:10.1016/j.epsl.2007.09.001)
91. Lesparre N, Gibert D, Marteau J, Komorowski JC, Nicollin F, Coutant O. 2012 Density muon radiography of La Soufrière of Guadeloupe volcano: comparison with geological, electrical resistivity and gravity data. *Geophys. J. Int.* **190**, 1008–1019. (doi:10.1111/j.1365-246X.2012.05546.x)
92. Jourde K, Gibert D, Marteau J, De Bremond d'Ars J, Komorowski JC. 2016 Muon dynamic radiography of density changes induced by hydrothermal activity at the La Soufrière of Guadeloupe volcano. *Sci. Rep.* **6**, 1–12. (doi:10.1038/srep33406)
93. Marteau J, De Bremond d'Ars J, Gibert D, Jourde K, Ianigro JC, Carlus B. 2017 DIAPHANE: Muon tomography applied to volcanoes, civil engineering, archaeology. *J. Instrum.* **12**, C02008. (doi:10.1088/1748-0221/12/02/C02008)
94. Rosas-Carbajal M, Jourde K, Marteau J, Deroussi S, Komorowski JC, Gibert D. 2017 Three-dimensional density structure of La Soufrière de Guadeloupe lava dome from simultaneous muon radiographies and gravity data. *Geophys. Res. Lett.* **44**, 6743–6751. (doi:10.1002/2017GL074285)
95. Gibert D, Beauducel F, Déclais Y, Lesparre N, Marteau J, Nicollin F, Tarantola A. 2010 Muon tomography: plans for observations in the Lesser Antilles. *Earth Planets Space* **62**, 153–165. (doi:10.5047/eps.2009.07.003)
96. Jourde K, Gibert D, Marteau J, de Bremond d'Ars J, Gardien S, Girerd C, Ianigro JC, Carbone D. 2013 Experimental detection of upward going cosmic particles and consequences for correction of density radiography of volcanoes. *Geophys. Res. Lett.* **40**, 6334–6339. (doi:10.1002/2013GL058357)
97. D'Errico M *et al.* 2020 Muon radiography applied to volcanoes imaging: the MURAVES experiment at Mt. Vesuvius. *J. Instrum.* **15**, C03014. (doi:10.1088/1748-0221/15/03/C03014)
98. Lo Presti D *et al.* 2018 The MEV project: design and testing of a new high-resolution telescope for muography of Etna Volcano. *Nucl. Instrum. Methods Phys. Res. Sect. A* **904**, 195–201. (doi:10.1016/J.NIMA.2018.07.048)

99. Lo Presti D, Riggi F, Ferlito C, Bonanno DL, Bonanno G, Gallo G, La Rocca P, Reito S, Romeo G. 2020 Muographic monitoring of the volcano-tectonic evolution of Mount Etna. *Sci. Rep.* **10**, 11351. (doi:10.1038/s41598-020-68435-y)
100. Tanaka HKM, Uchida T, Tanaka M, Takeo M, Oikawa J, Ohminato T, Aoki Y, Koyama E, Tsuji H. 2009 Detecting a mass change inside a volcano by cosmic-ray muon radiography (muography): first results from measurements at Asama volcano, Japan. *Geophys. Res. Lett.* **36**, L17302. (doi:10.1029/2009GL039448)
101. Tanaka HKM. 2019 Japanese volcanoes visualized with muography. *Phil. Trans. R. Soc. A* **377**, 20180142. (doi:10.1098/rsta.2018.0142)
102. Le Gonidec Y, Rosas-Carbajal M, de Bremond d'Ars J, Carlus B, Ianigro JC, Kergosien B, Marteau J, Gibert D. 2019 Abrupt changes of hydrothermal activity in a lava dome detected by combined seismic and muon monitoring. *Sci. Rep.* **9**, 3079–3087. (doi:10.1038/s41598-019-39606-3)
103. Tanaka HKM, Miyajima H, Kusagaya T, Taketa A, Uchida T, Tanaka M. 2011 Cosmic muon imaging of hidden seismic fault zones: rainwater permeation into the mechanical fractured zones in Itoigawa–Shizuoka Tectonic Line, Japan. *Earth Planet. Sci. Lett.* **306**, 156–162. (doi:10.1016/j.epsl.2011.03.036)
104. Nomura Y *et al.* 2020 Pilot study of eruption forecasting with muography using convolutional neural network. *Sci. Rep.* **10**, 5272. (doi:10.1038/s41598-020-62342-y)
105. Goodfellow I, Pouget-Abadie J, Mirza M, Xu B, Warde-Farley D, Ozair S, Courville A, Bengio Y. 2020 Generative adversarial networks. *Commun. ACM* **63**, 139–144. (doi:10.1145/3422622)
106. Litjens G, Kooi T, Bejnordi BE, Setio AAA, Ciompi F, Ghafoorian M, van der Laak JAWM, van Ginneken B, Sánchez CI. 2017 A survey on deep learning in medical image analysis. *Med. Image Anal.* **42**, 60–88. (doi:10.1016/j.media.2017.07.005)
107. Hochreiter S, Schmidhuber J. 1997 Long short-term memory. *Neural Comput.* **9**, 1735–1780. (doi:10.1162/neco.1997.9.8.1735)
108. Rudin C. 2019 Stop explaining black box machine learning models for high stakes decisions and use interpretable models instead. *Nat. Mach. Intell.* **1**, 206–215. (doi:10.1038/s42256-019-0048-x)
109. Tanaka HKM, Uchida T, Tanaka M, Shinohara H, Taira H. 2010 Development of a portable assembly-type cosmic-ray muon module for measuring the density structure of a column of magma. In *Earth, planets and space*, pp. 119–129. Berlin, Germany: Springer.
110. Yasui M, Koyaguchi T. 2004 Sequence and eruptive style of the 1783 eruption of Asama Volcano, central Japan: a case study of an andesitic explosive eruption generating fountain-fed lava flow, pumice fall, scoria flow and forming a cone. *Bull. Volcanol.* **66**, 243–262. (doi:10.1007/s00445-003-0308-8)
111. Tanaka HKM. 2015 Muographic mapping of the subsurface density structures in Miura, Boso and Izu peninsulas, Japan. *Sci. Rep.* **5**, 8305. (doi:10.1038/srep08305)
112. Kueppers U, Scheu B, Spieler O, Dingwell DB. 2005 Field-based density measurements as tool to identify preeruption dome structure: set-up and first results from Unzen volcano, Japan. *J. Volcanol. Geotherm. Res.* **141**, 65–75. (doi:10.1016/j.jvolgeores.2004.09.005)
113. Hale AJ. 2008 Lava dome growth and evolution with an independently deformable talus. *Geophys. J. Int.* **174**, 391–417. (doi:10.1111/j.1365-246X.2008.03806.x)
114. Kusagaya T. 2017 *Reduction of background noise in muographic images for detecting magma dynamics in an active volcano*. Tokyo, Japan: University of Tokyo. See https://repository.dl.itc.u-tokyo.ac.jp/?action=repository_action_common_download&item_id=52347&item_no=1&attribute_id=14&file_no=1.
115. Tanaka HKM. 2020 Development of the muographic tephra deposit monitoring system. *Sci. Rep.* **10**, 14820. (doi:10.1038/s41598-020-71902-1)
116. Bonneville A *et al.* 2019 Borehole muography of subsurface reservoirs. *Phil. Trans. R. Soc. A* **377**, 20180060. (doi:10.1098/rsta.2018.0060)